IRAQI
Academic Scientific Journals

Investigation of the impact of utilizing PCM into a coil in a single-pass air heater (experimental study)

Zeina Ahmed Mohammed[1], Ahmed Mustaffa Saleem[1]

[1]Northern Technical University, Engineering Technical College of Mosul, Cultural Group Street, Mosul, Iraq

ABSTRACT

This study aims to design, build, and assess the SAH's performance with an integrated enhanced phase-change material (PCM) absorber storage system. Using materials found locally, two single-pass solar air heaters were designed and produced for this study. The first solar heater was made without phase change material (Conventional SAH), and the second included PCM by adding paraffin wax to the coil tube (Improved SAH). In February, March, and April of 2024, real - results were carried out on the air heaters in Mosul city, Iraq. At a mass flow rate of 0.0147 kg/s, the experiments were conducted with and without a PCM system. As opposed to the first case without PCM, the study's findings indicated that the air temperature outside of the heater increased significantly in the second case with (the addition of paraffin wax). The highest recorded outlet temperatures in February, March, and April for both cases were (39.5, 50.7 °C), (49.4,58.9°C), and (57.4,70.6°C). To compare the efficiencies of the SAHs for both instances (Conventional and Improved), the efficiency of the improved SAH is higher than the efficiency of conventional SAH, such as (48.1% and 68.32 %), (58.6% and 72.8%), and (67.1% and 86.47%) in February, March, and April.

1. Introduction

Renewable energy is widely considered a viable way to mitigate the negative impacts of climate change and dwindling fossil fuel reserves. Solar power has received widespread attention as a renewable energy source mainly due to its abundant availability and sustainability. However, several challenges remain to be overcome, including the variability of solar energy due to weather conditions, the high costs associated with the initial setup and maintenance of solar infrastructure, and the need for efficient energy storage systems to ensure a steady power supply. Additionally, integrating solar power into existing energy grids presents technical and regulatory challenges that must be addressed to ensure reliability and efficiency.[1] Solar power has received widespread attention as a renewable energy source mainly due to its abundant availability and sustainability [1]. Solar heaters capture the sun's energy and use it to heat air for various purposes, whether drying or simply warming a space. However, low-tech and inexpensive solar air heating has the potential to curb energy consumption, which is a significant contributor to greenhouse gas emissions when traditional fossil fuels are used. Solar air heating systems can mitigate climate change by reducing reliance on conventional heating methods that typically burn fossil fuels.[1] Solar air heaters are broadly classified into glazed and unglazed types: Glazed collectors feature glass cover plates that allow sunlight transmission while minimizing heat loss and are highly efficient [2]. On the other hand, unglazed collectors work without any cover materials; hence, their performance could be better due to exposure to ambient conditions. Unglazed collectors are used in pool heating applications where cold water temperatures work well with them since they do not have covers and are exposed directly to outdoor conditions [3]. Using an air solar heater delivers an achievable and financially efficient resolution to reheat air in diverse contexts, including but not limited to space heating, drying processes, and ventilation mechanisms [1]. By exploiting solar energy, there is a decrease in reliance on conventional heating techniques, reducing energy expenses and carbon emissions

One major hindrance to solar air systems is their low thermal efficiency, which sharply curtails their productivity and effectiveness. In light of this particular hindrance, scientists have taken many avenues to better the thermal efficiency of solar air heaters. The innovations explored encompass thermal

storage materials, enhancement of collector designs, and integration of Nanofluids [4].

PCMs are used as components in various solar thermal systems, such as solar water or air heating systems, solar cookers, greenhouses, and others [5]. This breakthrough stimulates further developments in solar air heating technology. Researchers have studied different materials and designs to boost efficiency and performance.

Fath et al. [6] illustrated that the melting point of PCM significantly affects heat transfer in a solar air conditioner. Specifically, the study looked at four different PCMs with varying melting points: 61°C, 51°C, 43°C, and 32°C. Their findings pointed to the superior efficiency of heaters with Tm values of 43°C and 51°C.

Matsunaga et al. [7] validated their solar air heater's performance within a passive ventilation system. This was done through actual building measurements and simulation modeling. The model showed good consistency as it accurately determined that the heat absorption capacity of the heater was 5057 J/K and also estimated the heat capacity value for surrounding components. A comparison between computed and measured values confirmed the model's reliability; it successfully depicted temperature changes that helped illustrate how effective the solar air heater was in heating incoming air, achieving approximately a 30°C increase.

Yassien et al. [8] investigated the performance of two different triple-pass solar air heater collectors. They examined these collectors' efficiency due to other modifications made in a detailed analysis. TPSAH-2 had a dual-pane glass cover and tube network below the absorber surface, while TPSAH-1 had only a single glass cover as an alternative collector. In controlled winter experiments under constant weather conditions, it was found that TPSAH-2 outperformed TPSAH-1 at various air mass flow rates, reaching an optimum efficiency of 80.2% as opposed to 73.4% for TPSAH-1.

Abd et al. [9] investigated a Compound Parabolic Concentrator (CPC) using a flat plate receiver model. They discovered that increasing the speed at which water flows through the system reduces water temperature; this, in turn, increases the collector efficiency of the CPC system. The change in solar radiation levels from January to March did not significantly affect overall levels, with March having the highest intensity, peaking between 12 and 1 PM hours daily.

Zulkifle et al. [10] studied the application of V-groove absorber designs in a single-pass collector to

improve the efficiency of air-based solar collectors. The performance implications are assessed by comparing two cover designs: glass and Fresnel lens. Theoretical modelling and numerical simulations demonstrated that the collector fitted with a Fresnel lens achieved a much higher efficiency of 71.18% compared to the glass-covered collection, which only achieved an efficiency of 54.10%, while subjected to 755 W/m2 of solar irradiation.

Ahmadkhani et al. [11] aimed to investigate the performance of Triple-Channel, Double-Pass Solar Air Heaters (DPSAHs) in different situations. They looked into thermal and thermohydraulic characteristics by varying air mass flow rates (ranging from 0.01 to 0.025 kg/s), reflux ratios (from 0.1 to 1), and different recycling patterns. They also explored how inserting a matrix between absorber plates and glass covers affected DPSAH under various radiation levels. The outcome was quite interesting: using downhill recycling with an elevated matrix led to thermal efficiency spiking up to an unexpected 79%.

Abdullah et al. [12] studied the performance enhancement of solar air heaters through a single pass. He focused on introducing external reflectors as supplementary components to SAH coupled with a proper air distribution system, guide vanes, and stacked aluminum cans as tabulators. An experimental study tested various plate layouts: without cans, plain cans, and different features, including wrapped ones with reflectors and airflow rates ranging between 0.02 and 0.05 kg/s.

Chabane et al. [13] investigated the significant impact of longitudinal fins on improving heat transmission and promoting uniform fluid flow in solar air heaters. This finally optimizes the thermal efficiency of the heaters. He experimented to analyze the thermal efficiency of the heater. He used a solar air heater with a single-pass system and installed five longitudinal fins below the absorber plate. The fins serve the goal of enhancing heat transfer and promoting uniform fluid flow throughout the channel. Mothana et al. [14] showed that double glass covers yield positive results by enlarging the surface area of the absorber on two trapezoidal double-pass solar air heaters (DPSAH). Examining the compelled and inherent airflow was essential to the experimental configuration. Packed beds were used in DPSAH-1 to evaluate the efficacy of the heaters above the absorber surface. DPSAH-2 was run similarly but without the higher flow rate. Furthermore, employing natural convection to run the systems improves efficiency. When exposed to forced convection and natural convection at lower air mass transfer rates, the DPSAH-1 and DPSAH-2 achieve maximum efficiencies of 81% and 67%, respectively. The temperature difference between forced and natural convection is noticeable.

Chii-Dong Ho et al. [15] enhanced solar air heaters by conducting theoretical and practical examinations of their operation. The study's objective was to improve the rate of convective heat transfer by employing the recycling process and investigating the impact of the wire mesh on augmenting turbulence. The double-pass flat-plate solar air heaters, equipped with wire mesh packing, demonstrated much superior collector efficiency compared to alternative setups at various recycling ratios and mass flow rates. This exemplifies the effectiveness of this design in enhancing heat transfer efficiency.

Salah M. Salih et al. [16] evaluated the thermal efficiency of a double-pass solar air heater (DP-SAH) that utilizes rectangular capsules filled with paraffin wax, which acts as a phase change material (PCM). This study used computational and experimental assessments to evaluate the system's efficiency during the charging and discharging operations. An artificial sunshine simulator, a projector, was used to replicate natural sunlight indoors and conduct experimental studies. The system underwent testing at three distinct solar irradiation levels (625, 725, and 825 W/m2) and airflow speeds (0.6, 0.9, 1.2, 1.5, and 1.8 kg/min). The results indicated that increased airflow velocities decreased paraffin's melting point and prolonged the melting process's duration.

Al-Juamily et al. [17] investigated the effectiveness of a solar drying system in Iraq for fruit and vegetable preservation. The system consisted of a solar collector, a drying cabinet, and an air fan. The solar collector had a surface area of 2.4 square meters, a single glass cover, and V-corrugated absorption plates. The drying cabinet was designed to fit different types of fruits and vegetables; its walls were made using aluminum plates, with one side fixed securely with a glass plate.

2. Experimental work

2.1 Experimental setup design and construction

Figure 1 shows the conventional and improved SAH collectors. This figure provides a more detailed description of the traditional SAH, which uses 20 mm thick wool sheets for insulation, a wooden box measuring 1.20 m x 0.8 m, and a 1mm thick plate. The current model is a single-glazed system with a height above the absorption panel of 7.5cm. The glass used is 6 mm thick.

Figure 1 also shows the improved SAH; this collector's dimensions are 1.2mm long and 0.8m wide, and the collector uses 20mm thick crock insulation material. Heat-absorbing plates with a thickness of 1 mm are also used. The constructed SAH was a single glass collector located 7.5 cm above the absorber plate and was a commercially available glass plate with a thickness of 6 mm. This model is a modified version of SAH. It is integrated with copper coils infused with PCM. This model uses paraffin wax in the coil. The copper tube is about 1 mm thick, 12mm in inner diameter, and outer diameter 15mm.

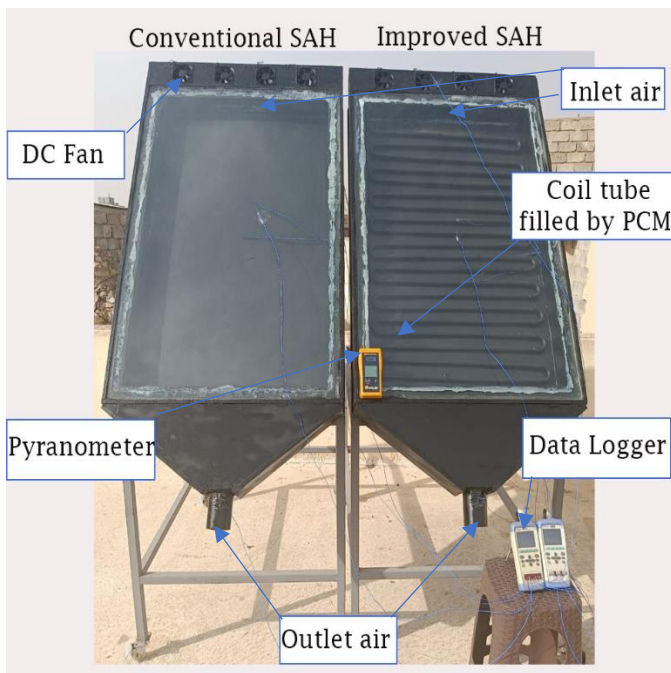The inlet ports of both SAHs are equipped with 4 DC fans to maintain air circulation in the proposed system.

Figure1: conventional and improved SAH collectors

2.1.1. Latent heat storage of PCM

Table (1) illustrates the physical and thermal properties of paraffin wax (PCM), standard parameters for commercial paraffin waxes used in this study. The amount of paraffin wax used to fill the coil tube is 1000 g. The tube is filled with paraffin wax to 85% of its volume for safety. Filling the tube 100% with wax leads to thermal expansion that exerts pressure on the tube, reduces heat transfer efficiency, and causes

mechanical stress that may damage the tube and increase the risk of explosion.

Table 1. Physical Properties of Paraffin Wax.

Properties of paraffin wax	Value
Melting temperature	58-60 °C
Heat storage capacity	250 kJ/kg
Density solid	(at 25°C) 880 kg/m²
Density liquid	(at 80°C) 760 kg/m²
Specific heat capacity	2 kJ/kg. K
Heat conductivity	0.2 W/m. K
Volume expansion	12.5%
Flash point	>180 °C
Max. operation temperature	70°C

3. Experimental setup sensor

Many thermocouples are employed to ascertain the temperature changes within the constructed SAH. These sensors encompass various temperature measurements, such as those at the airflow's inlet, outlet, and exit points. Figure 2 shows a schematic diagram of the installation of thermocouples in traditional and improved SAH.

These parameters were measured at ambient temperature. Table 2 provides a thorough representation using precise and accurate instruments, including information regarding the types of devices and the locations where sensors are installed.
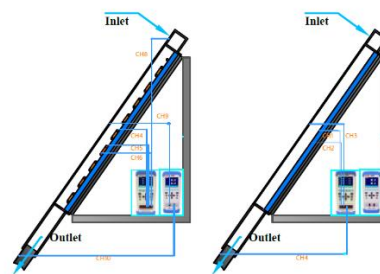

Figure 2: Schematic thermocouple installation location diagram and the data logger connection.

Table 2: Specifications of equipment sensor devices.

Equipment	Specification
Anemometer	AP- 816B
Thermocouples	k-type (10 in number)
Temperature indicator	8,2 channels data logger
Solar power meter	Seaward SS200R Solar Irradiance Meter

The collected data were compared to the thermometer readings to ensure that all thermocouples had accurate readings. Both devices provide measurements for frozen water placed in a metal container and subjected to a heat source gradually and by examination, as shown in Figure 3.
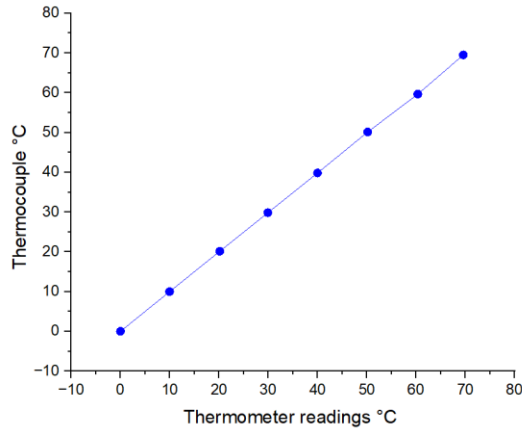

Figure 3: Calibration of Thermocouples.

4. The Experimental Setup

The experiments in this study were conducted outdoors Situation. Two solar air heaters (SAH with PCM and SAH without PCM) were developed locally; they were built in Mosul City in Iraq (latitude 36°340000 " N and longitude 43.130001° " E). The two collectors' directions are in the South and inclined 55 degrees to horizontal. The experimental test began at 9:10 a.m. and was discovered and recovered at 4:00 p.m. (local time). Both systems have been operated for several days in February, March, and April 2024 to supply the air mass flow rates of 0.0147kg/s with both SAH (Traditional and Improved). Critical data, including inlet temperature, absorption plate

temperature, glass transition temperature, paraffin temperature, outlet temperature, and environmental parameters, were measured for 5 minutes and recorded in the energy. This data was used for further analysis of thermodynamics and thermal efficiency.

5. Calculation of thermal performance of SAH collector

The absorber converts the solar energy to heat, which is then transferred to the working fluid through the heat exchange process between them. As a result, the amount of useful energy has been evaluated as [7,18]:

$$Qu = \dot{m} * Cp * \Delta T \qquad (1)$$

The thermal performance of the SAH collector (η_{th}) can be obtained as the ratio of useful energy to the solar energy that reached the aperture area [5]:

$$\eta_{th} = \frac{Q_u}{Q_i} \qquad (2)$$
Where:

$$Q_i = I * A_c \qquad (3)$$

The mass flow rate of the air ($\dot{m}$) through the heater can be calculated by the following equation [17]:

$$\dot{m} = \rho_{air} * A_t * V_{air}$$

Therefore, the thermal efficiency of a solar air heater can be specified using the following formula [14]:

$$\eta th = \frac{\dot{m} * Cp * (Tout - Tin)}{I * Ac} \qquad (4)$$

4. Results

Fig. 4 illustrates the behaviors of measured incident solar radiation concerning daylight hours for a particular day of these three months (February, March, and April). These days have been chosen to be 12 February, 5 March, and 2 April, where the air circulation condition's air mass flow rate has been fixed at 0.0147 kg/s. The figure shows that the maximum solar radiation value occurred in April because, in April, the angle of the sun's rays is more

direct compared to February and March, resulting in increased solar radiation intensity. From the behaviors of incident solar radiation in Fig. 3, it is evident that there is a substantial difference in their values, especially in February. The maximum values for those three months were recorded as 817 W/m²,959 W/m², and 1003 W/m² in February, March, and April, respectively. Moreover, the values of incident solar radiation in March at 9 AM and 5 PM are higher than those in February and March due to the time of sunrise and sunset being earlier and later, respectively, compared with February and March.
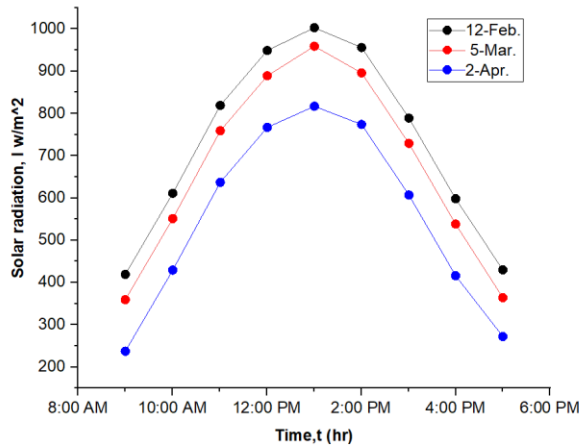
of traditional SAH is nearly equal to 38.5 °C in February, 49°C in March, and 57.4 April °C.

Figure 6 (b) shows that the temperature difference rises gradually until it reaches its peak value at 1 PM. The temperature difference increases after 9 AM until it reaches its peak value at 1 PM in February, March, and noon in April, and then it starts to reduce after these times.

Figure 6 (c) displays the variation of useful heat energy (Qu) in a solar air heater, noted on February 12, March 5, and April 2, 2024; the maximum values for these three months are 293 W, 392.9 W, and 449.14 W, respectively.
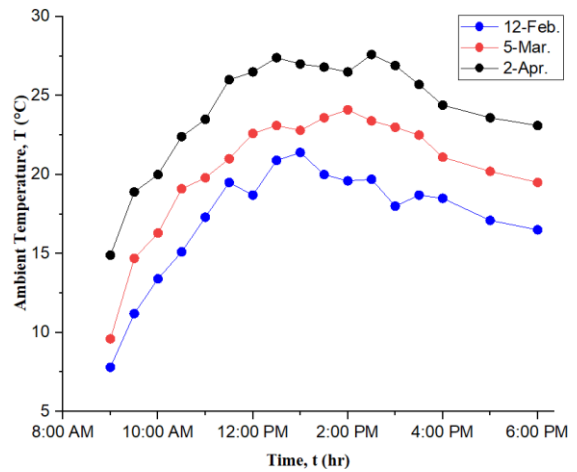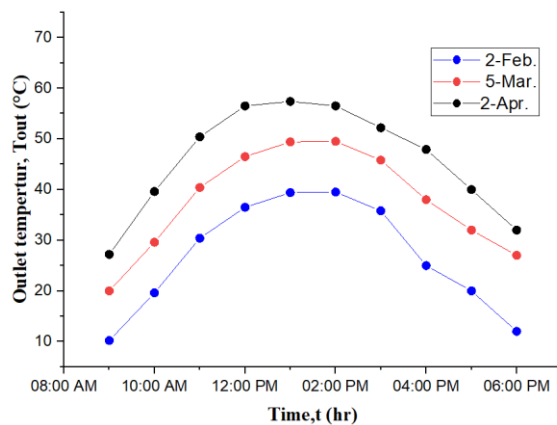

Figure 4: Profiles of I_T in terms of daylight hours on 12th Feb, 5th Mar, and 2nd April for $\dot{m}$= 0.0147 kg/s

Figure 5: Ambient temperature variation on 12 Feb, 5th Mar, and 2nd April (2024).

Figure 5 shows the ambient temperature or the temperature entering the two systems during the three days: 12 February, 5 March, and 2 April 2024. We conclude that the temperature on the 2nd of April has a maximum temperature value. The results show it has the highest temperature at one o'clock in the afternoon, measuring 27 °C on 2 April, 23.6 C on 5 March, and 21 °C on 12 February.

Figure 6 shows variations of outlet temperature, temperature difference, and useful energy in the experiment for traditional SAH. Fig. 6. (a) shows the variations of T_{out} for the traditional experiment; it is evident that T_{out} begins to increase after 9 AM until it achieves T_{out} max at 1 PM, and then it starts to reduce after those times; Tout max Fig. 6 (a) has also been obtained in April because the peak value of incident solar radiation has been recorded in April., T_{out}, max
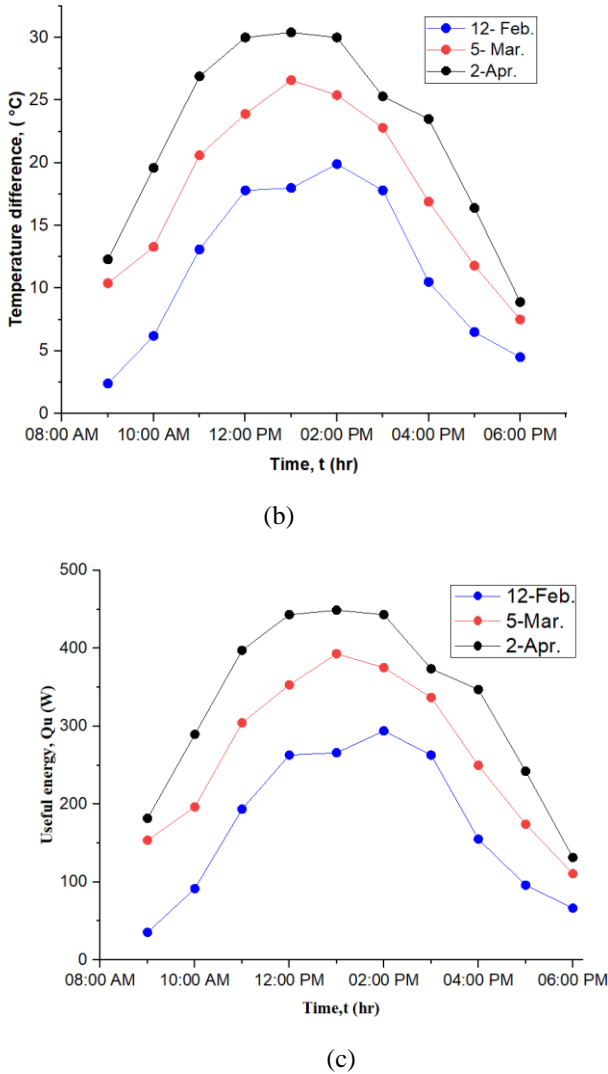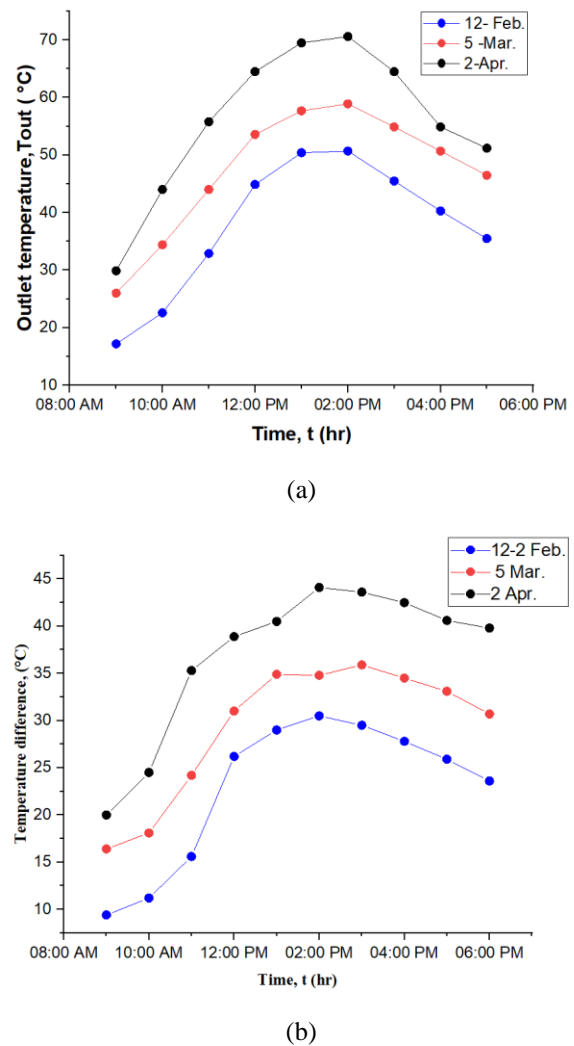

(a)

103

(b)

(c)

Figure 6: Variations of (a) T_{out}, (b) temperature difference, and (c) Q_u concerning daylight hours for traditional SHA on 12th February, 5th March, and 2nd April for $\dot{m}$= 0.0147 kg/s.

The variations of outlet temperature, temperature difference, and useful energy in the experiment of improved SHA are shown in Figure 7. (a) shows the variations of T_{out} for the traditional experiment; it is evident that Tout begins to increase after 9 AM until it achieves Tout, max at 1 PM, and then it starts to reduce after those times, T_{out}, max in Figure 7 (a) has also been obtained in April because the peak value of incident solar radiation has been recorded in April.,

T_{out}, max of improved SAH is nearly equal to 50.7°C on 12 February,58C on 5 March, and 70.6C in April.

Figure 7 (b) shows that the temperature difference rises gradually until it reaches its peak value at 1 PM. The temperature difference increases after 9 AM until it reaches its peak value at 1 PM in February, March, and noon in April, and then it starts to reduce after these times.

Figure 7 (c) displays the variation of useful heat (Qu) in a solar air heater, noted on February 12, March 5, and April 2, 2024; the maximum values for these three months are 471.8W, 589.5 W and 683.5W, respectively.
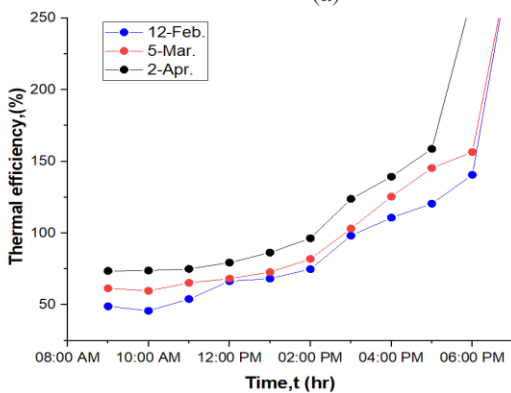

(a)

(b)

104
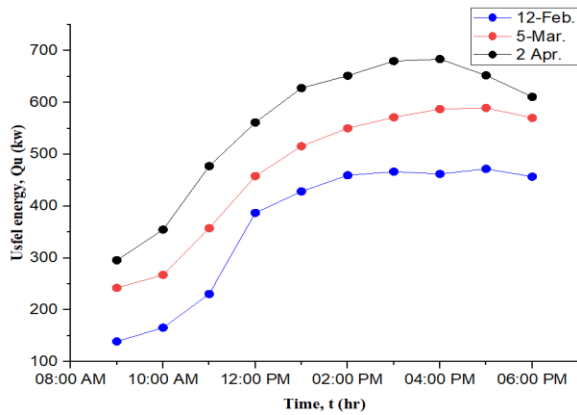
(c)

Figure 7: Variations of (a) Tout, (b) temperature difference, and (c) Q_u concerning daylight hours for improved SHA on 12th February, 5th March, and 2nd April for $\dot{m}$= 0.0147 kg/s.
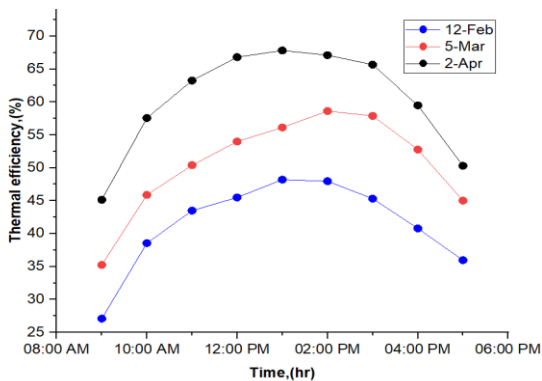
(a)

(b)

Figure 8: variations of η_{th} concerning daylight hours for both (a)traditional SHA and (b) improved SHA on 12th February, 5th March, and 2nd April for $\dot{m}$= 0.0147kg/s.

Figure 8 (a) and (b) show the variations of thermal efficiency concerning the local time of two different types of SAHs. These figures show that the thermal efficiency increases at 12:00–13:00 h and then decreases in the afternoon. Fig. 8 (a) shows that the maximum efficiency obtained is 48.19%, 58.6%, and 67.1% for traditional SAH for 12 Feb., 5 Mar., and 2 April, respectively. Fig.8 (b) shows the maximum efficiency between 11:30 h and 13:30 h for both types of SAHs. The maximum efficiency obtained for three days, 12 Feb., 5 Mar, and 2 April, was 68.32%, 72.8% and 86.47%, respectively.

5. Conclusions

The SAH integrated with PCM containers as a latent heat storage medium was studied experimentally when mass flow rates were 0.0147 kg/s. The instantaneous thermal efficiency of SAH was studied with and without PCM for three months: February, March, and April. Generally, instantaneous efficiency is higher in the case of heaters with PCM. The instantaneous efficiency of SAH with PCM was 68.32 % in February, 72.8% in March, and 86.47 % in April, which improved compared to without PCM, which was 48.1 % in February, 58.6 % in March and 67.1 % in April. Also, the outlet temperature was increased in the case of the heater with PCM, which recorded the maximum temperature for February, March, and April are (50.7, 58.9, and 70.6 °C), respectively. The heater's maximum temperature without PCM is (39.5, 49.4, and 57.4 °C).

References

[1] Sharol, A. F., Razak, A., Majid, Z. a. A., Azmi, M. a. A., Tarminzi, M., Ming, Y., Zakaria, Z., Harun, M. A., Fazlizan, A., & Sopian, K. (2022). Effect of thermal energy storage material on double-pass solar air heater performance with cross-matrix absorber. Journal of Energy Storage, 51, 104494. https://doi.org/10.1016/j.est.2022.104494

[2] Farzan, H., & Zaim, E. H. (2023). Study on the thermal performance of a new combined perforated Metallic/Asphalt solar air heater for heating Applications: An experimental study. Solar Energy, 249, 485–494. https://doi.org/10.1016/j.solener.2022.12.008

[3] Li, B., & Zhai, X. (2017). Experimental investigation and theoretical analysis on a mid-temperature solar collector/storage system with composite PCM. Applied Thermal Engineering, 124, 34–43. https://doi.org/10.1016/j.applthermaleng.2017.06.002

[4] Karthikeyan, A., Nimay, K., Dinesh, C., Jayaprabakar, J., & Jacob, A. (2023). Performance enhancement of solar thermal systems using phase change materials- a review. Materials Today: Proceedings. https://doi.org/10.1016/j.matpr.2023.01.109

[5] Mehla, N., & Yadav, A. (2015). Experimental analysis of the thermal performance of evacuated tube solar air collector with phase change material for sunshine and off-sunshine hours. International Journal of Ambient Energy, 38(2), 130–145. https://doi.org/10.1080/01430750.2015.1074612

[6] Fath, H. E. (1995). Transient analysis of thermosyphon solar air heater with built-in latent heat thermal energy storage system. Renewable Energy, 6(2), 119–124. https://doi.org/10.1016/0960-1481(94)00050-g

[7] Matsunaga, J., Kikuta, K., Hirakawa, H., Mizuno, K., Tajima, M., Hayashi, M., & Fukushima, A. (2021). An assessment of heating load reduction by a solar air heater in a residential passive ventilation system. Energies, 14(22), 7651. https://doi.org/10.3390/en14227651.

[8] Yassien, H. N. S., Alomar, O. R., & Salih, M. M. M. (2020). Performance analysis of triple-pass solar air heater system: Effects of adding a net of tubes below absorber surface. Solar Energy, 207, 813–824. https://doi.org/10.1016/j.solener.2020.07.041

[9] Maher, H., Alomar, O. R., Ali, F. A., & Salih, M. M. M. (2020). Experimental study of compound parabolic concentrator with flat plate receiver. Applied Thermal Engineering, 166, 114678. https://doi.org/10.1016/j.applthermaleng.2019.114678

[10] Zulkifle, I., Al-Waeli, A. H., Ruslan, M. H., Ibarahim, Z., Othman, M., & Sopian, K. (2018). Numerical investigation of V-groove air-collector performance with changing cover in Bangi, Malaysia. Case Studies in Thermal Engineering, 12, 587–599. https://doi.org/10.1016/j.csite.2018.07.012

[11] Ahmadkhani, A., Sadeghi, G., & Safarzadeh, H. (2021). An in-depth evaluation of matrix, external upstream, and downstream recycles on a double pass flat plate solar air heater efficacy. Thermal Science and Engineering Progress, 21, 100789. https://doi.org/10.1016/j.tsep.2020.100789

[12] Abdullah, A., Amro, M., Younes, M., Omara, Z., Kabeel, A., & Essa, F. (2020). Experimental investigation of single pass solar air heater with reflectors and turbulators. Alexandria Engineering Journal, 59(2), 579–587. https://doi.org/10.1016/j.aej.2020.02.004

[13] Chabane, F., Moummi, N., & Benramache, S. (2014). Experimental study of heat transfer and thermal performance with longitudinal fins of solar air heater. Journal of Advanced Research, 5(2), 183–192. https://doi.org/10.1016/j.jare.2013.03.001

[14] Salih, M. M. M., Alomar, O. R., & Yassien, H. N. S. (2021). Impacts of adding porous media on the double-pass solar air heater performance under natural and forced air circulation processes. International Journal of Mechanical Sciences, 210, 106738. https://doi.org/10.1016/j.ijmecsci.2021.106738

[15] Ho, C., Chang, H., Lin, C., Chao, C., & Tien, Y. (2015). Analytical and Experimental Studies of Wire Mesh Packed Double-Pass Solar Air Heaters under Recycling Operation. Energy Procedia, 75, 403–409. https://doi.org/10.1016/j.egypro.2015.07.404

[16] Salih, S. M., Jalil, J. M., & Najim, S. E. (2019). Experimental and numerical analysis of double-pass solar air heater utilizing multiple capsules PCM. Renewable Energy, 143, 1053–1066. https://doi.org/10.1016/j.renene.2019.05.050

[17] Al-Juamily, K. E., Khalifa, A. J. N., & Yassen, T. A. (2007). Testing the performance of a fruit and vegetable solar drying system in Iraq. Desalination, 209(1–3), 163–170. https://doi.org/10.1016/j.desal.2007.04.026

[18] Kabeel, A., Hamed, M. H., Omara, Z., & Kandeal, A. (2018). Influence of fin height on the performance of a glazed and bladed entrance single-pass solar air heater. Solar Energy, 162, 410–419. https://doi.org/10.1016/j.solener.2018.01.037

Nomenclature:

A_c solar collector surface area, m²
A_s exit air cross-section area, m²
$\dot{m}$ air mass flowrate, kg/s
C_p specific energy, kJ/kg. K
Q_u useful energy, W
V air velocity, m²/s
T_{amb} ambient temperature,° C
T_m Melting temperature

Greek Symbols:

ρ air density, kg/m³
η_{th} efficiency

Subscripts

PCM   phase change material
SAH   Solar Air Heater
amb   Ambient
(TPSAH)   Two triple-pass solar air heater